PCCP

RSC Publishing

PAPER

View Article Online
View Journal | View Issue

Cite this: *Phys. Chem. Chem. Phys.*, 2013, **15**, 14624

Effect of alkyl chain length and anion species on the interfacial nanostructure of ionic liquids at the Au(111)–ionic liquid interface as a function of potential

Hua Li,[a] Frank Endres[b] and Rob Atkin*[a]

Received 11th June 2013,
Accepted 10th July 2013

DOI: 10.1039/c3cp52421c

www.rsc.org/pccp

Colloid probe atomic force microscopy (AFM) force measurements are used to elucidate the effect of variation in the cation alkyl chain length and the anion species on IL nanostructure at Au(111) surfaces as a function of potential. Four ionic liquids (ILs) are examined: 1-ethyl-3-methylimidazolium tris(pentafluoroethyl)trifluorophosphate ([EMIM] FAP), 1-butyl-3-methylimidazolium tris(pentafluoroethyl)-trifluorophosphate ([BMIM] FAP), 1-hexyl-3-methylimidazolium tris(pentafluoroethyl)trifluorophosphate ([HMIM] FAP) and 1-butyl-3-methylimidazolium iodide ([BMIM] I). The step-wise force–distance profiles show the ILs adopt a multilayered morphology, with stronger near surface structure present at more biased potentials. The results suggest that the innermost (interfacial) layer is enriched in counter ions strongly bound to the Au(111) surface. For ILs with FAP^- anions, the cations in the interfacial layer at negative potentials pack more neatly than the anions at positive potentials, and thus more effectively template structure in subsequent layers. [BMIM] FAP has the weakest interfacial structure. [EMIM] FAP has stronger interfacial structure because the imidazolium rings of $[EMIM]^+$ cations in the interfacial layer are orientated towards the Au(111) surface, and this more parallel orientation is favourable for templating structure. [HMIM] FAP is more strongly structured than [BMIM] FAP because the longer cation alkyl chain increases solvophobic interactions which lead to better defined near surface structure. The response of [BMIM] I to changes in potential is opposite to that of the FAP^- ILs. [BMIM] I interfacial nanostructure is stronger at positive potentials, because I^- anions pack more neatly at the Au(111) surface than $[BMIM]^+$ cations, which templates stronger structure in subsequent layers.

Introduction

Ionic liquids (ILs) are composed entirely of ions and are usually liquid at temperatures less than 100 °C.[1–3] Due to their low melting point,[4,5] low volatility,[6] thermal stability,[7] intrinsic conductivity[8] and wide electrochemical windows,[9] ILs exhibit advantages over conventional molecular liquids in various applications, including electrochemistry,[10–12] and lubrication,[13–20] amongst many others. Interest in ILs for electrochemical studies is primarily a consequence of their nonvolatility and wide electrochemical windows; ILs can sustain higher voltages in electrochemical cells than conventional molecular solvents,[21] making electrochemical processes that occur at relatively high potentials possible.[22]

ILs are more structured in the bulk and at surfaces than molecular liquids,[23] because they are subject to a range of strong cohesive interactions including Coulombic, van der Waals, hydrogen bonding and solvophobic forces.[24,25] Three regions can be identified close to IL–solid, IL–liquid or IL–gas interfaces.[25] The *interfacial (innermost) layer* is composed of ions in direct contact with the other phase. The *bulk phase* refers to the bulk liquid, which often has a layered, sponge-like morphology of interpenetrating polar and apolar regions.[25,26] The *transition zone* is the region over which the strong interfacial layer structure decays to the bulk morphology, and is usually a few nanometres wide.

IL–electrode interfacial structure has traditionally been studied using electrochemical impedance spectroscopy (EIS). The effect of alkyl chain length on the electrical double layer was investigated using 1-alkyl-3-methylimidazolium chloride and 1-alkyl-3-methylimidazolium tetrafluoroborate on different electrodes.[27,28] Thinner double layers were found when the

[a] *Centre for Advanced Particle Processing and Transport, The University of Newcastle, Callaghan, NSW 2308, Australia. E-mail: Rob.Atkin@newcastle.edu.au*
[b] *Institute of Electrochemistry, Clausthal University of Technology, Arnold-Sommerfeld-Str. 6, 38678 Clausthal-Zellerfeld, Germany*

cation alkyl chain was shorter, but the level of interfacial structure and the orientation of the ions in the double layer could not be determined. The effect of varying the anion was studied using a series of ILs with $[EMIM]^+$ and $[BMIM]^+$ cations.[29,30] For ILs with halide anions, the double layer thickness increases with the anion size. However, for ILs with more complex anions, the capacitance curves could not be sufficiently deconvoluted to enable rigorous interpretation. In any case, only averaged, macroscopic information can be derived from EIS results, meaning that there is no direct link between the ion structure and the features of the capacitance curves, and the interfacial nanostructure. Additionally, there is considerable variation in published EIS data,[29] which complicates analysis.

Theoretical descriptions of the IL–electrode interface using mean field theory[31,32] and molecular dynamics and Monte Carlo simulations[21,33–42] have both predicted ''bell-'' and ''camel-'' shaped capacitance curves, consistent with experimental data. The simulations also reveal oscillating ion density profiles consistent with layered ion arrangements near the electrode surface. Despite this progress, simulations fail to reproduce layered structures at neutral surfaces, as they underestimate IL–surface interactions as well as bulk alkyl chain clustering,[25,43,44] and theoretical descriptions have not elucidated the effect of ion species and orientation. Thus, further studies are required to elucidate the influence of ion structure (*e.g.* cation alkyl chain length and anion species) on the nanostructure of IL–electrode interfaces. We seek to probe these issues in this manuscript.

IL structure in the interfacial layer and transition zone has been investigated at various solid surfaces by atomic force microscopy (AFM).[45–47] The interfacial layer has the most ordered structure, and is enriched in cations for anionic surfaces and anions for cationic surfaces.[25] Strong structure in the interfacial layer templates ion arrangements in the transition zone, which can extend several ion pair diameters from the interface before the bulk morphology is reached. More recently, we have used AFM force curve measurements and *in situ* scanning tunnelling microscopy (STM) to investigate the surface and near surface nanostructure of the IL–Au(111) electrode interface. IL interfacial nanostructure is strongly affected by the surface potential.[25,48–50] The composition of the interfacial layer varies from anion-enriched (at positive potentials) to cation-enriched (at negative potentials), and stronger near surface structures are found at higher potentials due to stronger electrostatic interactions. Force curves allow inferences to be made about the orientation of the ions adsorbed near the surface. Reconstruction of Au(111)$(22 \times \sqrt{3})$ has been imaged using STM for a single-crystalline Au(111) surface in contact with various ILs at negative potentials.[51–54] This reconstruction is a consequence of cation adsorption, as the reconstructed worm-like structure depends on the length of the alkyl chain.[55]

In this paper the effect of variation in the cation alkyl chain length and the anion species on IL nanostructure at polarized Au(111) surfaces is elucidated. The effect of changing the cation alkyl chain length is investigated using [EMIM] FAP, [BMIM] FAP, and [HMIM] FAP, while the influence of anion species is investigated by comparing results for [BMIM] I with [BMIM] FAP. A silica colloid probe is employed for this investigation rather than a sharp AFM tip, because the larger well-defined interaction area afforded by the probe increases measurement sensitivity[56] and reduces the possibility that an isolated surface asperity produces unrepresentative force data. Comparison of results obtained from this set of ILs elucidates routes to control interfacial IL structure normal to the interface as a function of potential, which will allow electrochemical systems to be optimised.

Experimental

All ILs used in this study were purchased from Merck in high purity grade (purity > 99%, water content < 100 ppm). The chemical structure, density, molecular volume, ion pair diameter and melting points are shown in Table 1. Atomically smooth Au(111) surfaces (a gold film of ~150 nm thickness on mica) were purchased from Agilent technologies.

Colloid probe force measurements were acquired using a Digital Instruments NanoScope IV Multimode AFM with an EV scanner in contact mode. A silica probe (5 μm diameter, Bangs Laboratories Inc.) was attached to a tipless rectangular cantilever (model CSC12, Mikromasch, Tallinn, Estonia) using Araldite epoxy. Over the course of this investigation, three cantilevers from the same batch were used. The spring constants (0.5 ± 0.05 N m^{-1}) were determined using the thermal vibration method following the procedure of Sader.[57] The ILs were held in an AFM fluid cell, sealed with a silicone O-ring to prevent water ingression. The water content was lower than 300 ppm after the AFM measurement. The tip was cleaned immediately prior to use by careful rinsing in Milli-Q water, drying under nitrogen and irradiation with ultraviolet light for 40 min.

The procedures used to setup the AFM electrochemical cell are exactly as described in ref. 25. Atomically smooth Au(111) surface were used as both the working electrode and the solid substrate for force measurements. Three Au(111) surfaces of similar roughness (0.3 nm for a 5 μm × 5 μm region) were used in the measurements. A thin cylindrical strip of Cu metal and 0.25 mm Pt wire were used as the counter and ''quasi'' reference electrodes, respectively. The electrochemical windows (the difference between the cathodic and anodic limits) of the ILs were obtained from cyclic voltammetry measured in the AFM electrochemical cell. The values are listed in Table 1.

For all systems and surface potentials, force measurements were performed by moving the surface towards the colloid probe and recording the cantilever deflection dependence on separation. The force curves were collected over 30 nm at a scan rate of 0.1 Hz. Deflection *vs.* separation data were converted to force *vs.* apparent separation curves using standard methods.[58] By convention, the region of constant compliance is used to define the zero separation in an AFM experiment. However, it is possible that strongly adsorbed species resist ''squeeze out'' even at high force, and the probe contacts an adsorbed layer rather than the solid surface at zero separation. To account for this, the distance between the probe and the surface is referred to as the ''apparent separation''.[20]

Table 1 Abbreviation, structure, melting points (T_m), density (ρ),[a] ion pair diameter (d_m),[b] and electrochemical window (E) of the ILs used

Ionic liquid	Abbrev.	Structure	T_m (°C)	ρ (g cm^{-3})	d_m (nm)	E (V)
1-Ethyl-3-methylimidazolium tris(pentafluoroethyl)trifluorophosphate	[EMIM] FAP	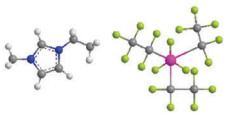	−1	1.72	0.81	−2.0 to +2.4
1-Butyl-3-methylimidazolium tris(pentafluoroethyl)trifluorophosphate	[BMIM] FAP	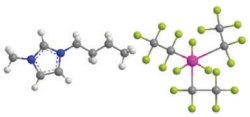	3	1.63	0.84	−1.9 to +2.5
1-Hexyl-3-methylimidazolium tris(pentafluoroethyl)trifluorophosphate	[HMIM] FAP	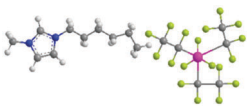	−14	1.56	0.87	−2.0 to +2.3
1-Butyl-3-methylimidazolium iodide	[BMIM] I	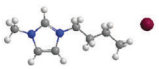	−58	1.44	0.67	−1.2 to +0.8

[a] The melting point and density values were from the manufacturer.[59] [b] The diameter of ion pairs were estimated by assuming a cubic packing geometry.[60] Carbon atoms are shaded grey, nitrogen are blue, hydrogen are white, fluorine are yellow, phosphorous are pink and iodide are red.

Repeat experiments revealed that the features of the force curves were constant. Every system and surface potential was studied over three or more separate experiments.

Results and discussion

AFM force–distance profiles for [EMIM] FAP, [BMIM] FAP, [HMIM] FAP and [BMIM] I (*cf.* Table 1) confined between a silica colloid probe (5 μm) and an Au(111) electrode surface are investigated at different applied potentials within each IL's electrochemical window (Fig. 1–4). The major features for the four ILs examined are similar at all potentials. The force profiles consist of a series of steps at discrete separations; each step corresponds to an interfacial IL layer. The force required to rupture a layer corresponds to the maximum height of each step, and is referred to as the ''rupture force'' or ''push-through force''. Because the roughness of the silica colloid probe[61] is substantially greater than that of the gold surface,[62] the measured forces are primarily a consequence of the Au(111) electrode.[45]

The nanostructure of many ILs is transformed from sponge-like[25,45] in the bulk to a flatter, more ordered, layered morphology by the presence of a smooth solid surface, analogous to surface induced sponge to lamellar phase transitions in aqueous surfactant systems.[63] For all systems and all potentials, push-through forces increase closer to the surface, indicating stronger structure. The width of each step is a consequence of the physical dimensions of the cation, the anion, or ion pairs confined between the probe and the surface. Thus, the widths of the steps in the force–distance profiles provide an indication of the ionic composition of interfacial layers, particularly closest to the surface. The magnitude of the push-through force reflects the degree of order in an ion layer, with higher force indicative of stronger order. In all systems, stronger forces are measured at higher biases, indicating that the ions in the layers are more ordered.

Of the FAP^- ILs, [BMIM] FAP has the weakest interfacial structure. The interfacial structure for this IL is described first, after which the more strongly structured [EMIM] FAP and [HMIM] FAP systems are discussed. Finally the interfacial nanostructure of [BMIM] I is presented, which reveals how interfacial structure changes when an inorganic anion is employed.

In Fig. 1(a) at 0 V, a series of steps are noted at discrete separations as the silica probe moves towards the Au(111) surface. No force is measured beyond ~5 nm, which indicates that the AFM is insensitive to the bulk nanostructure of [BMIM] FAP. As the probe moves closer to the surface, it encounters a weak layer at a separation of ~4.2 nm and pushes against it until a force of 0.02 nN is reached. Then the probe jumps ~0.9 nm before encountering another layer at ~3.3 nm from the interface. The process is repeated another three times with layers detected at 2.4 nm, 1.5 nm and 0.6 nm; the widths of the steps, except for the final one, are in accordance with the predicted [BMIM] FAP ion pair diameter of 0.84 nm determined from the bulk density (*cf.* Table 1). The magnitude of the push-through force increases with decreasing apparent separation, confirming that the layered structure becomes more pronounced with increasing confinement. This is consistent with previous experiment[23,25,45,64,65] and theoretical predictions.[66] When a potential (either positive or negative) is applied to the Au(111) surface, the force–distance behaviour is generally similar, with step-wise profiles obtained. Only the width of the final step decreases, and the push-through forces increase.

At 0 V, the width of the final step (~0.6 nm) is smaller than that of an ion pair (0.84 nm) but larger than the size of a $[BMIM]^+$ cation (0.35 nm) or a FAP^- anion (0.5 nm). This suggests that this layer is of mixed composition. The relatively low magnitude of force required to push through this layer (1.5 nN) indicates that the ions are not well ordered. This layer is likely slightly enriched in cations due to the negative charge on the silica probe and the amphiphilicity of $[BMIM]^+$.

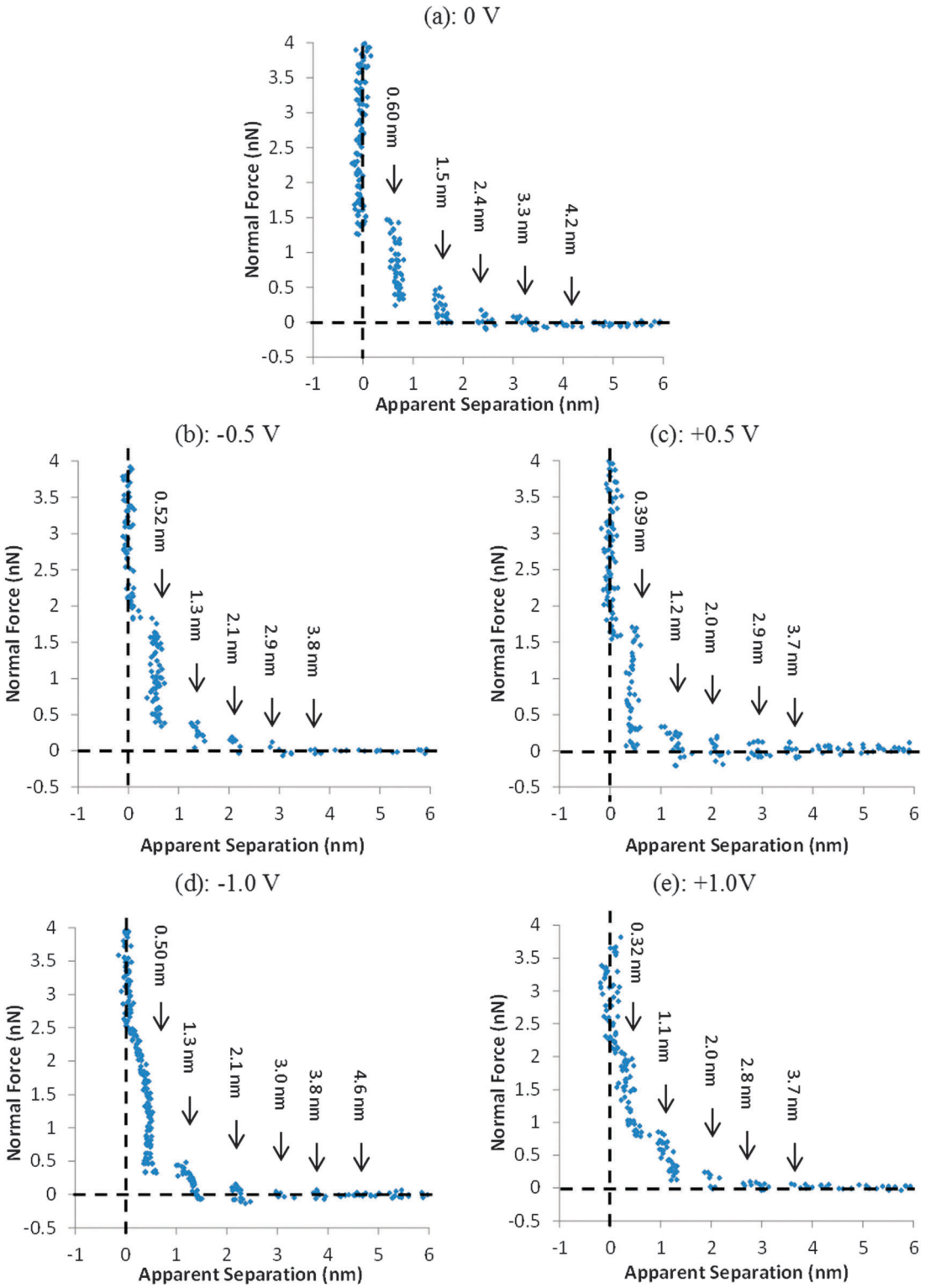

Fig. 1 Typical force *versus* apparent separation profile for a silica colloid probe approaching an Au(111) surface in [BMIM] FAP at: (a) 0 V, (b) −0.5 V, (c) +0.5 V, (d) −1.0 V and (e) +1.0 V.

Final steps of ~0.5 nm are detected at negative potentials (−0.5 V and −1.0 V), which are consistent with layers enriched with FAP^- anions. As it is physically unreasonable that ions of the same charge with the surface are enriched in the interfacial layer, this strongly suggests that the silica probe and the Au(111) surface are not in direct contact at zero separation. Rather, the closest approach in these experiments occurs when the silica probe contacts a cation-enriched layer bound to the

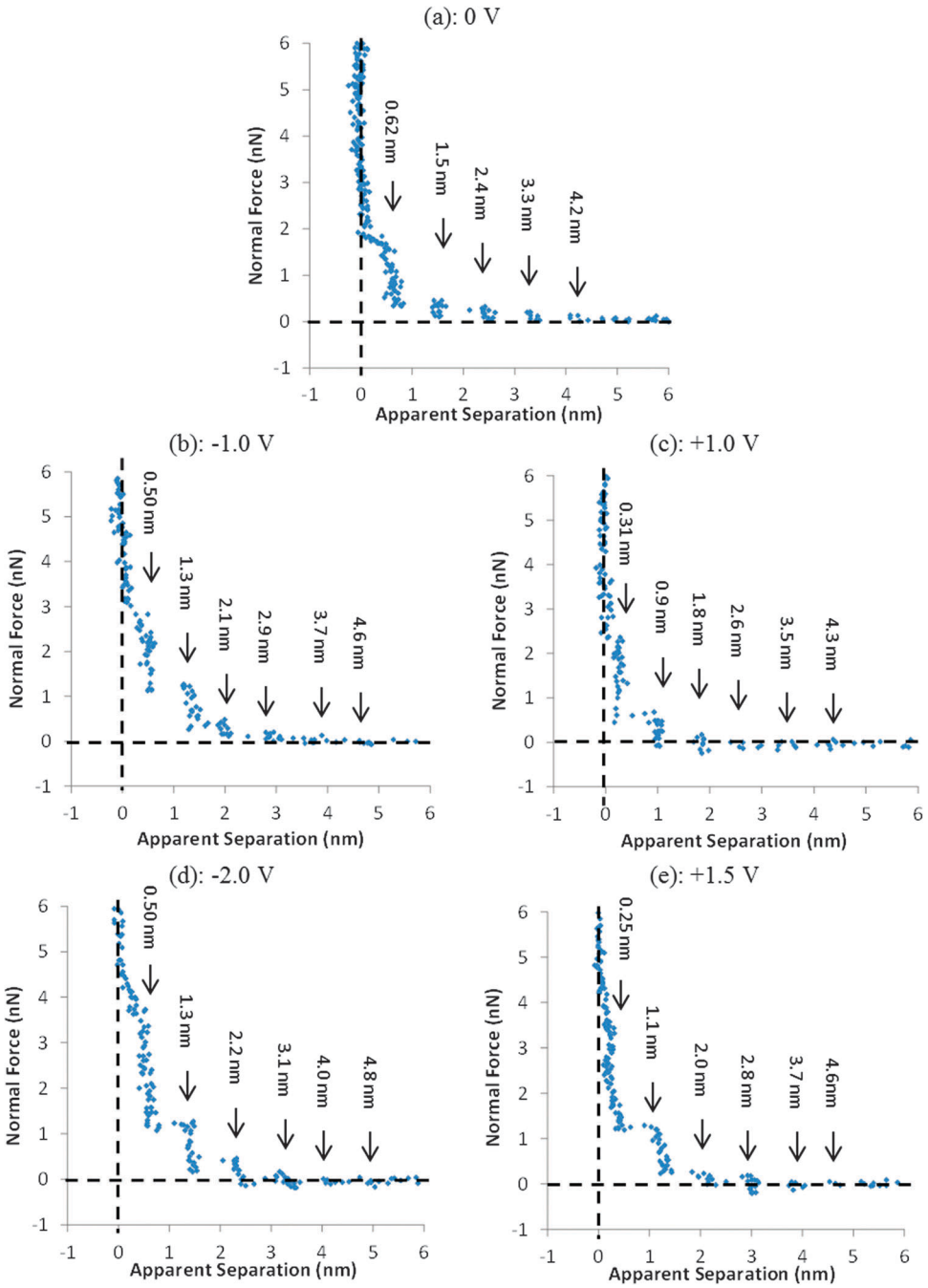

Fig. 2 Typical force *versus* apparent separation profile for a silica colloid probe approaching an Au(111) surface in [EMIM] FAP at: (a) 0 V, (b) −1.0 V, (c) +1.0 V, (d) −2.0 V and (e) +1.5 V.

Au(111) surface that is unable to rupture, *i.e.* the final step in the force curve corresponds to the probe pushing through the first transition zone layer, not the innermost (interfacial) layer, which remains in place up to high force. The force required to rupture this final step increases with potential, indicating stronger near surface structure.

At positive potentials, the final steps (~0.39 nm at +0.5 V and ~0.32 nm at +1.0 V) are close to the dimensions of $[BMIM]^+$ cations (~0.35 nm). Thus, at positive potentials there is an anion-enriched layer bound to the surface when the separation is zero, which remains in place up to high force. Like the results at negative potentials, higher forces are required to rupture the final step as potential is increased, due to stronger interfacial structure. The magnitude of the push-through force for the final step at positive potentials is similar to that obtained at negative potentials. This suggests that the level of order in the transition zone is similar at positive and at negative potentials for this IL.

Reducing the IL alkyl chain length from C_4 for [BMIM] FAP to C_2 for [EMIM] FAP slightly decreases the ion pair

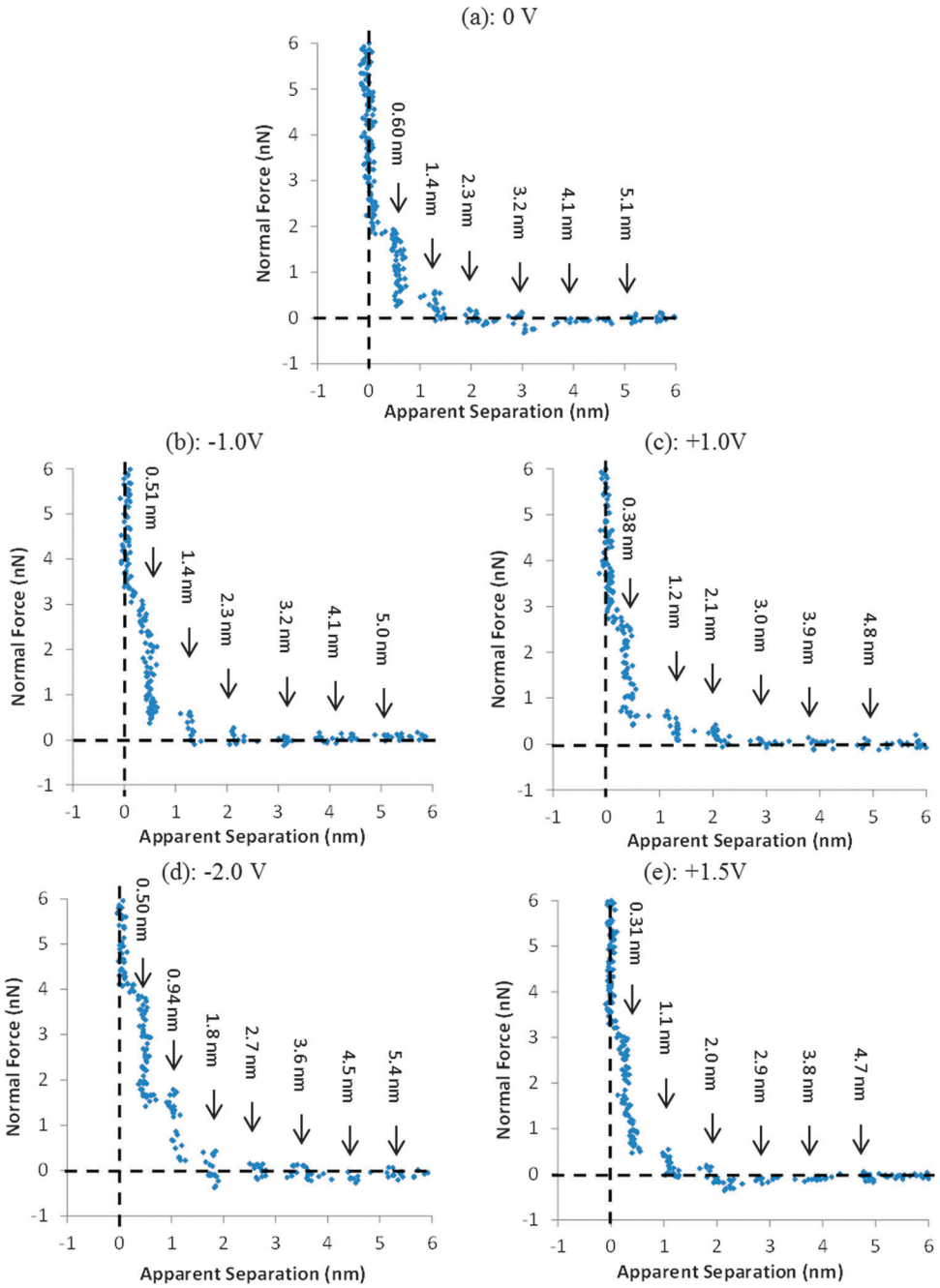

Fig. 3 Typical force *versus* apparent separation profile for a silica probe approaching an Au(111) surface in [HMIM] FAP at: (a) 0 V, (b) −1.0 V, (c) +1.0 V, (d) −2.0 V and (e) +1.5 V.

diameter, *cf.* Table 1. The step-wise force–distance profiles for [EMIM] FAP in Fig. 2 are similar to those for [BMIM] FAP in Fig. 1. Around five steps are found at 0 V and six steps are found at negative and positive potentials. The final step is ~0.62 nm at 0 V, ~0.50 nm at negative potentials, and ~0.30 nm at positive potentials, similar to the distances for [BMIM] FAP. The ionic composition of the layers is thus expected to be similar. Like [BMIM] FAP, the push-through forces increase with applied potential, but the magnitude of the push-through forces is higher for [EMIM] FAP, indicating stronger structures. This is likely because the $[EMIM]^+$ cations in the interfacial layer adopt an orientation more parallel to the Au(111) surface than the $[BMIM]^+$ cations,[67–69] and this well-formed layer effectively templates subsequent transition zone layers. However, at positive potentials, the magnitudes of the push-through forces for the two ILs are similar. This suggests that the interfacial layer is FAP^- enriched, and its structure and composition are unaltered by changing the alkyl chain at positive potentials, within the sensitivity of the measurement.

Increasing the alkyl chain length from C_4 for $[BMIM]^+$ to C_6 for $[HMIM]^+$ results in the number of transition zone layers and

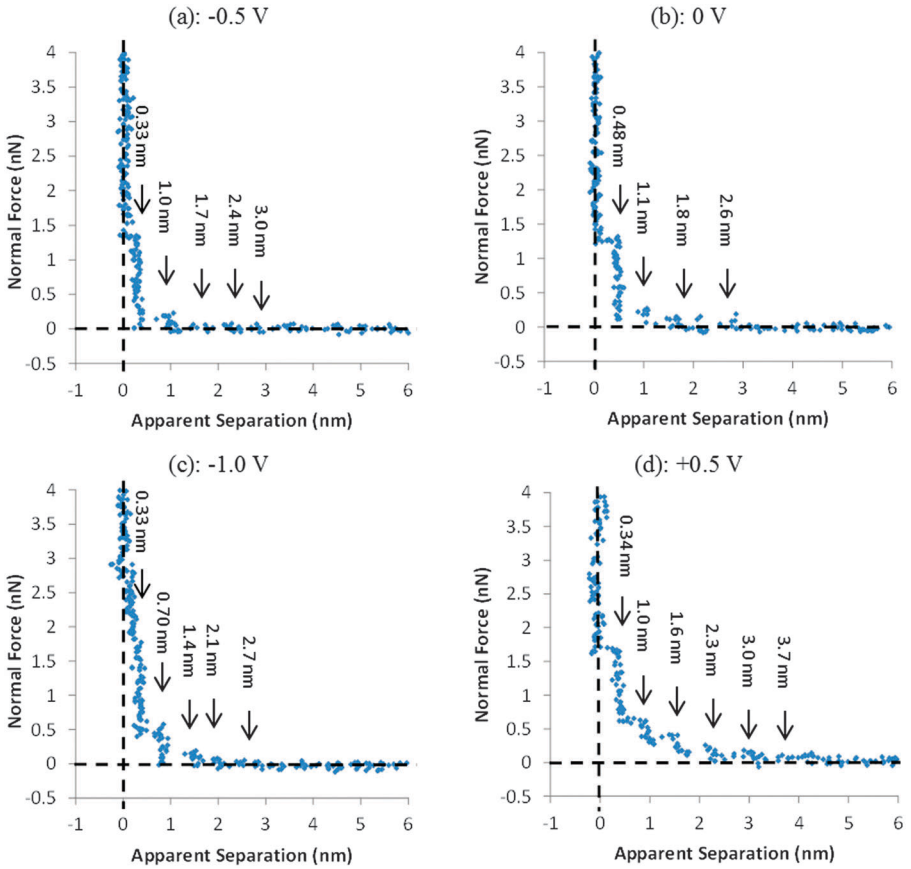

Fig. 4 Typical force *versus* apparent separation profile for a silica probe approaching an Au(111) surface in [BMIM] I at: (a) −0.5 V, (b) 0 V, (c) −1.0 V, and (d) +0.5 V.

the magnitude of the push-through forces increasing, *cf.* Fig. 3. At 0 V, five layers are noted, which increases to six–seven layers for biased surfaces. At the same potential, push-through forces for [HMIM] FAP are similar to [EMIM] FAP (and thus larger than [BMIM] FAP). These results indicate that the interfacial structure of [HMIM] FAP is stronger than [BMIM] FAP because increasing the cation alkyl chain length increases the strength of the solvophobic interactions, resulting in greater cohesive energy within the layers.[67] Thus, more layers are formed at the interface, and higher forces are required to rupture each layer.

For all three FAP^- ILs at positive potentials, the width of the final step becomes slightly thinner as the bias is increased. Although the difference is small, it is consistent across all FAP^- ILs investigated, and probably suggests a neater packing structure at the interface. A corresponding effect is not observed at negative potentials.

Experiments with [BMIM] I (Fig. 4) reveal how replacing the organic FAP^- anion with an inorganic anion (I^-) affects the interfacial structure as a function of surface potential. At all potentials except for +0.5 V, the number of steps in the force–distance profiles is reduced, compared to the FAP ILs, especially at 0 V, where only three–four layers are detected. The spacing between the steps in the force profiles is also more scattered, and the magnitude of the push-through forces is reduced. All of these differences are consistent with weaker interfacial structure. This could be a consequence of changing the anion from the large, charge-delocalized FAP^- to the small, charge-localized I^-. Alternatively, weaker structure could be due to the lower melting point of [BMIM] I compared to the FAP^- ILs (*cf.* Table 1). As the ions in [BMIM] I are more thermally activated than the FAP^- ILs at room temperature, this will disrupt solvophobic attractions between cation alkyl groups, and thus decrease the level of interfacial order.[46] The widths of the final steps for [BMIM] I are ~0.48 nm at 0 V, ~0.33 nm at negative potentials, and ~0.34 nm at +0.5 V. As the packing dimensions of the $[BMIM]^+$ (~0.35 nm) cation and I^- anion (~0.33 nm) are almost the same, it is impossible to comment on the composition of layers from step widths. However, based on electrostatic arguments and results for the other ILs, it is likely that the innermost (interfacial) layer is of mixed composition at 0 V, enriched in $[BMIM]^+$ cations at negative potentials and enriched in I^- anions at +0.5 V. The magnitude of the forces required to push through the layers increases with the potential, in line with results for FAP^- ILs, suggesting enhanced near surface structure.

In stark contrast to results obtained with FAP^- ILs, [BMIM] I has stronger interfacial structure at positive potentials than at negative potentials; the steps at +0.5 V are more pronounced than those at −0.5 V, and the forces required to push through corresponding layers are higher. These results suggest that the spherical shape and localized charge of I^- allow this anion to adsorb strongly to the Au(111) surface and arrange into a

well-ordered interfacial layer, which induces better ordering of ion pairs in subsequent layers, compared to FAP^-.

In a recent article the surface forces apparatus (SFA) was used to measure the force profiles for 1-butyl-3-methylimidazolium bis(trifluoromethylsulfonyl)imide ([BMIM] NTf_2) confined between a mica surface and a gold electrode as a function of potential.[70] At both positive and negative potentials, an attractive force was measured between ~3 nm and ~30 nm. We have measured attractive forces when trace water[71] or halide[50] was dissolved in the IL, but the authors state that the [BMIM] NTf_2 is electrochemically pure, so impurities would not seem to be the origin of the attraction. From fits to the force curves it was concluded that the IL was a dilute electrolyte in which the ions were only 0.003% dissociated. We cannot see any evidence for attractive forces in our data which is likely a consequence of the AFM being orders of magnitude less sensitive than the SFA;[70] we do not dispute that this long range force could be real. However, we offer an alternative explanation for the measured long range attraction based on IL interfacial nanostructure.

A variety of experimental techniques,[23,45,64,65,72–74] theoretical predictions[31,32] and simulations[21] have concluded that ILs become more ordered at a solid surface, and that this order increases with potential.[50,64,74] We have suggested that the bulk sponge structure present in many ILs is transformed to a more layered structure by the surface,[23] analogous to surface induced sponge to lamellar phase transitions observed for aqueous surfactant sponge phases.[63] These aqueous surfactant sponge phases also offer an explanation for the attractive forces measured for [BMIM] NTf_2 that does not require treating the IL as a weak electrolyte. Confinement induced sponge to lamellar transitions have been reported for sodium bis(2-ethylhexyl)sulfosuccinate–brine solutions confined between mica sheets using the SFA.[75] When the mica sheets were brought together from wide separation, a linear attractive force was measured from about 200 nm due to capillary condensation of the lamellar phase between the surfaces. This attractive force was used to extract the surface tension between the lamellar and sponge phases, which was similar to the surface tension between the lamellar phase and microemulsion interfaces, or lamellar and micelle interfaces. We contend that a similar effect is in operation for [BMIM] NTf_2. The physical dimensions of the IL sponge structure,[44] is about an order of magnitude lower than that of the aqueous surfactant sponge[76,77] and the range of the attractive force in the IL is also about 10 times less, which is structurally consistent. Experiments are currently underway to test this hypothesis using AFM and SFA.

Conclusions

The interfacial nanostructure of [EMIM] FAP, [BMIM] FAP, [HMIM] FAP and [BMIM] I at Au(111) surfaces has been investigated using colloid probe AFM normal force curve measurements. Ion arrangements vary significantly as a function of applied potential, with more pronounced structure detected at more positive or negative potentials. The force–distance profiles suggest an interfacial layer enriched in counterions which is strongly bound to the Au(111) surface and cannot be ruptured by the colloid probe.

For the ILs with FAP^- anions, push-through forces are higher at negative potentials than at positive potentials, indicating stronger interfacial structure. This means surface bound cations are more effective than FAP^- anions for inducing near surface structure. The influence of cation alkyl chain length on the push-through force is pronounced at negative potentials. Push-through forces for [BMIM] FAP are the lowest, indicating the weakest structure. [EMIM] FAP has stronger interfacial structure because the imidazolium rings of $[EMIM]^+$ cations in the interfacial layer are orientated more parallel to the Au(111) surface, which is favourable for templating structure, and [HMIM] FAP has stronger structure because the longer cation alkyl chain produces a stronger solvophobic force that increases the cohesive forces within layers. For FAP^- ILs at positive potentials, the push-through forces are similar, suggesting the layer is FAP^- enriched, and thus similarly effective for templating transition zone structure regardless of the cation alkyl chain length. When I^- replaces FAP^-, less interfacial layers are detected, especially at 0 V. Stronger structure is detected at positive potentials than at negative potentials, indicating an interfacial layer of I^- anions is more effective than $[BMIM]^+$ cations for templating transition zone structure.

These results suggest that the structure and composition of the interfacial layer can be tuned by the surface potential and the IL ion structure (*i.e.* the alkyl chain length and the anion species).

Acknowledgements

This research was supported by an ARC Discovery Project (DP120102708). RA thanks the ARC for a Future Fellowship. RA acknowledges useful discussion with Greg Warr, Mark Rutland and Susan Perkin regarding long range attractive forces in ILs. HL thanks Dr Grant Webber, Mr James Sweeney, Robert Hayes and Thomas Murphy for valuable discussions and suggestions.

References

1 T. Welton, *Chem. Rev.*, 1999, **99**, 2071–2083.
2 R. Hagiwara and Y. Ito, *J. Fluorine Chem.*, 2000, **105**, 221–227.
3 K. N. Marsh, J. A. Boxall and R. Lichtenthaler, *Fluid Phase Equilib.*, 2004, **219**, 93–98.
4 D. S. Silvester, *Analyst*, 2011, **136**, 4871–4882.
5 Q. Zhang, S. Zhang and Y. Deng, *Green Chem.*, 2011, **13**, 2619–2637.
6 R. D. Rogers, K. R. Seddon, Editors Ionic Liquids as Green Solvents: Progress and Prospects. (Proceedings of the 224th American Chemical Society Natl. Meeting held 18–22 August 2002 in Boston Massachusetts.) [In: ACS Symp. Ser., 2003, 856], 2003.
7 J. G. Huddleston, A. E. Visser, W. M. Reichert, H. D. Willauer, G. A. Broker and R. D. Rogers, *Green Chem.*, 2001, **3**, 156–164.

8 J. Vatamanu, O. Borodin, D. Bedrov and G. D. Smith, *J. Phys. Chem. C*, 2012, **116**, 7940–7951.
9 A. M. O'Mahony, D. S. Silvester, L. Aldous, C. Hardacre and R. G. Compton, *J. Chem. Eng. Data*, 2008, **53**, 2884–2891.
10 F. Endres, *ChemPhysChem*, 2002, **3**, 144–154.
11 M. Gorlov and L. Kloo, *Dalton Trans.*, 2008, 2655–2666.
12 S. Z. E. Abedin and F. Endres, *Acc. Chem. Res.*, 2007, **40**, 1106–1113.
13 C. Ye, W. Liu, Y. Chen and L. Yu, *Chem. Commun.*, 2001, 2244–2245.
14 B. S. Phillips and J. S. Zabinski, *Tribol. Lett.*, 2004, **17**, 533–541.
15 B. Bhushan, M. Palacio and B. Kinzig, *J. Colloid Interface Sci.*, 2008, **317**, 275–287.
16 M.-D. Bermúdez, A.-E. Jiménez, J. Sanes and F.-J. Carrión, *Molecules*, 2009, **14**, 2888–2908.
17 I. Minami, *Molecules*, 2009, **14**, 2286–2305.
18 S. Perkin, T. Albrecht and J. Klein, *Phys. Chem. Chem. Phys.*, 2010, **12**, 1243–1247.
19 J. Sweeney, F. Hausen, R. Hayes, G. B. Webber, F. Endres, M. W. Rutland, R. Bennewitz and R. Atkin, *Phys. Rev. Lett.*, 2012, **109**, 155502.
20 O. Werzer, E. D. Cranston, G. G. Warr, R. Atkin and M. W. Rutland, *Phys. Chem. Chem. Phys.*, 2012, **14**, 5147–5152.
21 M. V. Fedorov, N. Georgi and A. A. Kornyshev, *Electrochem. Commun.*, 2010, **12**, 296–299.
22 Y.-Z. Su, Y.-C. Fu, Y.-M. Wei, J.-W. Yan and B.-W. Mao, *ChemPhysChem*, 2010, **11**, 2764–2778.
23 R. Hayes, G. G. Warr and R. Atkin, *Phys. Chem. Chem. Phys.*, 2010, **12**, 1709–1723.
24 A. Ray, *Nature*, 1971, **231**, 313–315.
25 R. Hayes, S. Imberti, G. G. Warr and R. Atkin, *Phys. Chem. Chem. Phys.*, 2011, **13**, 3237–3247.
26 R. Hayes, S. Imberti, G. G. Warr and R. Atkin, *Phys. Chem. Chem. Phys.*, 2011, **13**, 13544–13551.
27 V. Lockett, R. Sedev, J. Ralston, M. Horne and T. Rodopoulos, *J. Phys. Chem. C*, 2008, **112**, 7486–7495.
28 M. T. Alam, M. M. Islam, T. Okajima and T. Ohsaka, *J. Phys. Chem. C*, 2008, **112**, 16600–16608.
29 V. Lockett, M. Horne, R. Sedev, T. Rodopoulos and J. Ralston, *Phys. Chem. Chem. Phys.*, 2010, **12**, 12499–12512.
30 C. Nanjundiah, S. F. McDevitt and V. R. Koch, *J. Electrochem. Soc.*, 1997, **144**, 3392–3397.
31 A. A. Kornyshev, *J. Phys. Chem. B*, 2007, **111**, 5545–5557.
32 K. B. Oldham, *J. Electroanal. Chem.*, 2008, **613**, 131–138.
33 J. Vatamanu, O. Borodin and G. D. Smith, *J. Am. Chem. Soc.*, 2010, **132**, 14825–14833.
34 S. A. Kislenko, I. S. Samoylov and R. H. Amirov, *Phys. Chem. Chem. Phys.*, 2009, **11**, 5584–5590.
35 S. K. Reed, O. J. Lanning and P. A. Madden, *J. Chem. Phys.*, 2007, **126**, 084704–084713.
36 M. V. Fedorov and A. A. Kornyshev, *Electrochim. Acta*, 2008, **53**, 6835–6840.
37 M. V. Fedorov and A. A. Kornyshev, *J. Phys. Chem. B*, 2008, **112**, 11868–11872.
38 G. Feng, J. S. Zhang and R. Qiao, *J. Phys. Chem. C*, 2009, **113**, 4549–4559.
39 S. Wang, S. Li, Z. Cao and T. Yan, *J. Phys. Chem. C*, 2009, **114**, 990–995.
40 N. Georgi, A. A. Kornyshev and M. V. Fedorov, *J. Electroanal. Chem.*, 2010, **649**, 261–267.
41 J. Vatamanu, O. Borodin and G. D. Smith, *J. Phys. Chem. B*, 2011, **115**, 3073–3084.
42 A. I. Frolov, K. Kirchner, T. Kirchner and M. V. Fedorov, *Faraday Discuss.*, 2012, **154**, 235–247.
43 T. L. Greaves, D. F. Kennedy, S. T. Mudie and C. J. Drummond, *J. Phys. Chem. B*, 2010, **114**, 10022–10031.
44 A. Triolo, O. Russina, H.-J. Bleif and E. Di Cola, *J. Phys. Chem. B*, 2007, **111**, 4641–4644.
45 R. Atkin and G. G. Warr, *J. Phys. Chem. C*, 2007, **111**, 5162–5168.
46 D. Wakeham, R. Hayes, G. G. Warr and R. Atkin, *J. Phys. Chem. B*, 2009, **113**, 5961.
47 R. Hayes, S. Z. E. Abedin and R. Atkin, *J. Phys. Chem. B*, 2009, **113**, 7049.
48 R. Atkin, N. Borisenko, M. Drüschler, S. Z. E. Abedin, F. Endres, R. Hayes, B. Huber and B. Roling, *Phys. Chem. Chem. Phys.*, 2011, **13**, 6849.
49 T. Carstens, R. Hayes, S. Z. E. Abedin, B. Corr, G. B. Webber, N. Borisenko, R. Atkin and F. Endres, *Electrochim. Acta*, 2012, **82**, 48.
50 R. Hayes, N. Borisenko, B. Corr, G. B. Webber, F. Endres and R. Atkin, *Chem. Commun.*, 2012, **48**, 10246–10248.
51 R. Atkin, N. Borisenko, M. Drüschler, S. Z. E. Abedin, F. Endres, R. Hayes, B. Huber and B. Roling, *Phys. Chem. Chem. Phys.*, 2011, **13**, 6849–6857.
52 R. Atkin, S. Z. E. Abedin, R. Hayes, L. H. S. Gasparotto, N. Borisenko and F. Endres, *J. Phys. Chem. C*, 2009, **113**, 13266–13272.
53 L. G. Lin, Y. Wang, J. W. Yan, Y. Z. Yuan, J. Xiang and B. W. Mao, *Electrochem. Commun.*, 2003, **5**, 995–999.
54 G.-B. Pan and W. Freyland, *Chem. Phys. Lett.*, 2006, **427**, 96–100.
55 Y.-Z. Su, J.-W. Yan, M.-G. Li, Z.-X. Xie, B.-W. Mao and Z.-Q. Tian, *Z. Phys. Chem.*, 2012, **226**, 979–994.
56 O. Werzer, G. G. Warr and R. Atkin, *Langmuir*, 2011, **27**, 3541–3549.
57 J. E. Sader, J. W. M. Chon and P. Mulvaney, *Rev. Sci. Instrum.*, 1999, **70**, 3967–3969.
58 J. Ralston, I. Larson, M. W. Rutland, A. A. Feiler and M. Kleijn, *Pure Appl. Chem.*, 2005, **77**, 2149–2170.
59 Merck, Ionic liquid safety data sheet, http://www.merckmillipore.com.
60 L. Jones and P. Atkins, *Chemistry: Molecules, Matter and Change*, 4th edn, 2000.
61 O. Werzer, E. D. Cranston, G. G. Warr, R. Atkin and M. W. Rutland, *Phys. Chem. Chem. Phys.*, 2012, **14**, 5147–5452.
62 R. Atkin, S. Z. E. Abedin, R. Hayes, L. H. S. Gasparotto, N. Borisenko and F. Endres, *J. Phys. Chem. C*, 2009, **113**, 13266–13272.

63 W. A. Hamilton, L. Porcar, P. D. Butler and G. G. Warr, *J. Chem. Phys.*, 2002, **116**, 8533–8546.
64 M. Mezger, H. Schroder, H. Reichert, S. Schramm, J. S. Okasinski, S. Schoder, V. Honkimaki, M. Deutsch, B. M. Ocko, J. Ralston, M. Rohwerder, M. Stratmann and H. Dosch, *Science*, 2008, **322**, 424–428.
65 R. G. Horn, D. F. Evans and B. W. Ninham, *J. Phys. Chem.*, 1988, **92**, 3531.
66 K. Shimizu, A. Pensado, P. Malfreyt, A. A. H. Padua and J. N. C. Lopes, *Faraday Discuss.*, 2012, **154**, 155–169.
67 R. Atkin, S. Z. E. Abedin, R. Hayes, L. H. S. Gasparotto, N. Borisenko and F. Endres, *J. Phys. Chem. C*, 2009, **113**, 13266.
68 B. D. Fitchett and J. C. Conboy, *J. Phys. Chem. B*, 2004, 20255.
69 J. B. Rollins, B. D. Fitchett and J. C. Conboy, *J. Phys. Chem. B*, 2007, **111**, 4990.
70 M. A. Gebbie, M. Valtiner, X. Banquy, E. T. Fox, W. A. Henderson and J. N. Israelachvili, *Proc. Natl. Acad. Sci. U. S. A.*, 2013, DOI: 10.1073/pnas.1307871110.
71 J. A. Smith, O. Werzer, G. B. Webber, G. G. Warr and R. Atkin, *J. Phys. Chem. Lett.*, 2010, **1**(1), 64–68.
72 Y. Min, M. Akbulut, J. R. Sangoro, F. Kremer, R. K. Prud'homme and J. Israelachvili, *J. Phys. Chem. C*, 2009, **113**, 16445–16449.
73 S. Perkin, L. Crowhurst, H. Niedermeyer, T. Welton, A. M. Smith and N. N. Gosvami, *Chem. Commun.*, 2011, **47**, 6572–6574.
74 R. Hayes, N. Borisenko, M. K. Tam, P. C. Howlett, F. Endres and R. Atkin, *J. Phys. Chem. C*, 2011, **115**, 6855–6863.
75 D. A. Antelmi, P. Kékicheff and P. Richetti, *Langmuir*, 1999, **15**, 7774–7788.
76 D. Roux, M. E. Cates, U. Olsson, R. C. Ball, F. Nallet and A. M. Bellocq, *EPL*, 1990, **11**, 229.
77 C. Coulon, D. Roux and A. M. Bellocq, *Phys. Rev. Lett.*, 1991, **66**, 1709–1712.